Journal of Himalayan Earth Sciences Volume 58, No. 1, 2025 pp. 88-106

Geometry and Kinematics of the Gentle to Open Fault-propagation Fold having Four-way Dip Enclosure: Outcrop and Lineament Analysis of the Rois Anticline, Southern Kirthar Fold Belt, Pakistan

Aijaz Ali Halepoto[1,*] Muhammad Hassan Agheem[1], Asghar A. A. D. Hakro[1], Shabeer Ahmed[1,2], and Surriya Bibi Ahmedani[1,3]

[1]*Centre for Pure and Applied Geology, Faculty of Natural Sciences, University of Sindh, Jamshoro, Pakistan*

[2]*Oil and Gas Development Company Limited, Islamabad, Pakistan*

[3]*Government (Zubeda) Girls College, Hyderabad, College Education Department, Government of Sindh*

**Corresponding author: aijaz.halepoto@usindh.edu.pk*

Submitted date: 07/10/2024 Accepted date: 28/02/2025 Published online: 31/03/2025

Abstract

The Rois anticline is located in the Southern Kirthar Fold Belt, Pakistan, and it exhibits an ideal example of fault-related folding. In this study we analyzed outcrop and lineaments data to understand geometry, lineament distribution pattern and kinematics of the fault-propagation Rois anticline. The outcrop observations were supported with geometrical parameters determined through stereographic projections to understand geometry of the anticline. Outcrop observations indicated that the Rois anticline is about 6.5Km along and 02Km across strike, N-S trending, culminated anticline having steep eastern and gentle western limbs, exhibiting four-way dip enclosure. The anticline is bounded by emergent frontal thrust in the eastern limb and by tear fault (lateral ramp) along the northern part. Geometrical parameters, i.e. fold axis, axial plane, interlimb angle and fold vergence, indicated that the Rois anticline is an asymmetrical, doubly-plunging, inclined to upright, gentle to open and ESE-vergent fold. The lineaments were extracted automatically from Digital Elevation Models. The transverse and longitudinal lineaments are identified in the Rois anticline. Transverse lineaments occur in the culmination, indicating anticline has experienced outer-arc extension. The longitudinal lineaments are concentrated in hinge area of the Rois anticline, which indicate fold-parallel stretching in its high-strain parts. The lineaments are interpreted as fold-related axial fractures or minor faults associated with propagating fault. Emergent frontal thrust, fold asymmetry, steep eastern limb and longitudinal axial lineaments supports the model of fault-propagation fold. It is developed due to east-directed compressional stresses linked to the oblique collision of the Indian Plate and Afghan Block along the Ornach-Nal and Chaman plate boundary. The Rois anticline has accommodated localized coaxial strain partitioning, associated with regional pure shear.

Keywords: Geometry and kinematics; Fault-propagation fold; Four-way dip enclosure; Lineament analysis; Rois Anticline; Southern Kirthar Fold Belt

1. Introduction

Fault-propagation folds are fundamental structural elements in the fold belts across the world (Tavani et al., 2006; Jabbour et al., 2012; Butler et al., 2018). Understanding their geometry and kinematics is critical to reconstruct the regional tectonic history and evaluation of hydrocarbon traps (Mitra, 1990; Wu et al., 2023). They develop when displacement along a thrust fault is transformed into folding of the hanging-wall strata, thereby creating distinctive geometric patterns and kinematic relationships (Suppe and Medwedeff, 1990; Erslev and Mayborn, 1997). The fault-propagation folds are characterized by steep to overturned fore-limb and gentle back-limb (Mosar and Suppe, 1992; Jabbour et al., 2012). The geometry and kinematics of the fault-propagation folds has widely been studied, because they often form significant hydrocarbon traps and provide insights into the regional structural evolution (Suppe and Medwedeff, 1990; Mitra, 1990; Jadoon et al., 2015; Khattak et al., 2017; Jiang et al., 2020; Halepoto et al., 2023a).

Outcrop observations integrated with

lineaments extracted from satellite imagery may provide valuable insights regarding geometry and kinematics of fault-propagation folds. Lineaments are fractures developed during folding and post-folding modifications due to extension, tension or drag effects (Gupta, 2018; Wajid et al., 2021; Jadoon et al., 2024). Lineaments parallel to fold axis are called longitudinal or extensional lineaments. They are perpendicular to maximum stress axis and are developed due to extension or stretching in high-strain parts of a fold, such as fore-limb, hinges or growing tip of thrust fault. Lineaments perpendicular to fold axis are called transverse or tensional lineaments. They are parallel to maximum stress axis and are developed due to either outer-arc stretching or differential compression (Watkins et al., 2015; Watkins et al., 2019; Jadoon et al., 2024).

The lineament distribution pattern in the fault-propagation folds, their geometrical and kinematic significance, particularly in the context of the Kirthar Fold Belt, is poorly understood. The Rois anticline is located in the Southern Kirthar Fold Belt and it has well-preserved surface exposure and fold-fault relationship. Hence, it is an excellent structure to study the geometry and kinematics of the fault-propagation folds through outcrop and lineament analysis. Therefore, present study is aimed to understand the structural geometry and kinematics of the Rois anticline by using outcrop data and lineament interpretation. This study will not only contribute to the understanding of geometry and kinematics of the Rois anticline, but also provide broader implications for lineament distribution in the fault-propagation folds in the Southern Kirthar Fold Belt, and similar tectonic settings worldwide.

2. Regional Tectonic Background

The transpressional collision of the Indian Plate with the Afghan Block formed the Sulaiman Fold Belt (SFB) and Kirthar Fold Belt (KFB) on the northwestern margin of the Indian Plate (Bannert et al., 1992; Hinsch et al., 2019; Jadoon et al., 2020; Ghani et al., 2023) (Figure 1). The SFB and KFB are separated by the "Sibi Trough" (Sibi Foreland Basin). The KFB is southwestern continuation of regional Himalayan fold-thrust belt, and is located along the western boundary of the Southern Indus Basin, Pakistan. The deformation in the KFB was controlled by inversion of Mesozoic normal faults, which acted as basement ramps during folding and thrusting (Fowler et al., 2004; Hinsch et al., 2019; Ghani et al., 2023). Sedimentary sequences from Jurassic to Recent are well developed and exposed in the KFB (Hunting Survey Corporation, 1960; Thebo et al., 2023; Halepoto et al., 2023c). The Paleocene and younger rocks are exposed in the foreland KFB, whereas Mesozoic sequences are exposed in the hinterland of KFB (Hunting Survey Corporation, 1960; Hedley et al., 2001; Smewing et al., 2002b; Halepoto et al., 2023b). The hinterland Mesozoic sequences are overlain by Bela Ophiolites (Allemann, 1979; De Jong and Subhani, 1979; Sarwar, 1992). The hinterland of the KFB consists of "Kalat Anticlinorium (KA)", "Kalat Synclinorium (KS)", "Bela-Wazirstan Ophiolite Zone (BWOZ)", "Ornach-Nal-Chaman Fault Zone (ONCFZ)", "Khuzdar Knot", "Bela Ophiolites", "Porali Trough (PT)" and "Pab Range". The foreland of the KFB consists of "Mula-Bulan Range (MBR)", "Kirthar Range (KR)", "Karachi Embayment (KE)", "Sumbakh Uplift (SU)" and "Lakhra Uplift (LU)" (Figure 1) (Kazmi and Rana, 1982). The deformation of the foreland KFB is characterized by faster rates (~2.5 km/Ma) of orogenic growth and exhumation during end of the Miocene (between ~7 and 5Ma), which is older than Salt Range deformation (~4Ma) and younger than MBT development (~12Ma) (Ghani et al., 2021; Ghani et al., 2023). The post-Miocene (since ~5Ma) deformation of the foreland KFB is characterized by slower shortening rates (<1 km/Ma) (Ghani et al., 2023). The KFB is divided into two distinct zones, i.e. Northern Kirthar Fold Belt (NKFB) and Southern Kirthar Fold Belt (SKFB), based on along-strike variation in the structural style and shortening magnitudes (Figure 1). Northern Kirthar Fold Belt consists of passive-roof duplexes, which accommodate horizontal tectonic shortening of 30-40% (Banks and Warburton, 1986; Hinsch et al., 2019). Southern Kirthar Fold Belt consists of thin-skinned, imbricate-fan structural style, which accommodate horizontal tectonic shortening of about 15% (Ahmed and Ali, 1991; Schelling,

1999; Smewing et al., 2002a; Fowler et al., 2004; Halepoto et al., 2023b). The LU, SU, KE, Pab Range and PT are prominent tectonic elements of the SKFB (Figure 1). The anticlines in the foreland SKFB depicting generally N-S orientation of their fold axes. The internal anticlines of foreland SKFB are relatively broad and gentle, whereas, frontal anticlines have steep to overturned forelimbs, breached by emergent thrusts (Figure 2) (Schelling, 1999; Halepoto et al., 2022; Halepoto et al., 2023a). The Rois anticline (~6.5Km along and ~02Km across the strike) is located in the SU of SKFB, bounded by Surjan anticline in the east and gas-producing Hundi anticline in the west (Figure 1-2).

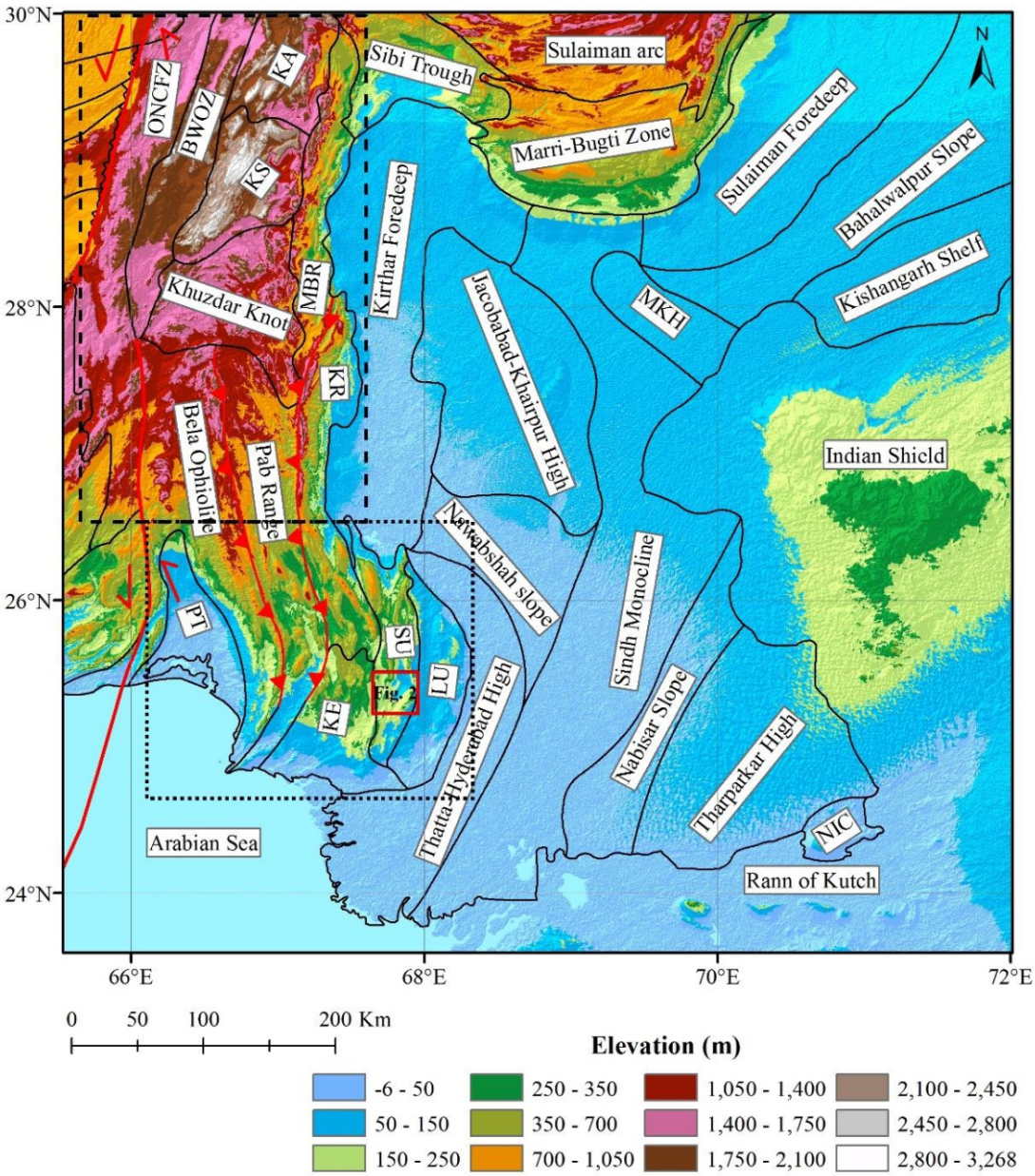

Fig. 1. Regional tectonic map, showing elements of the Southern Indus Basin, Kirthar and Sulaiman fold belts (After Kazmi and Rana, 1982). The SKFB and NKFB are demarcated with dotted and dashed rectangles respectively. The location of figure 2 is indicated with red square.

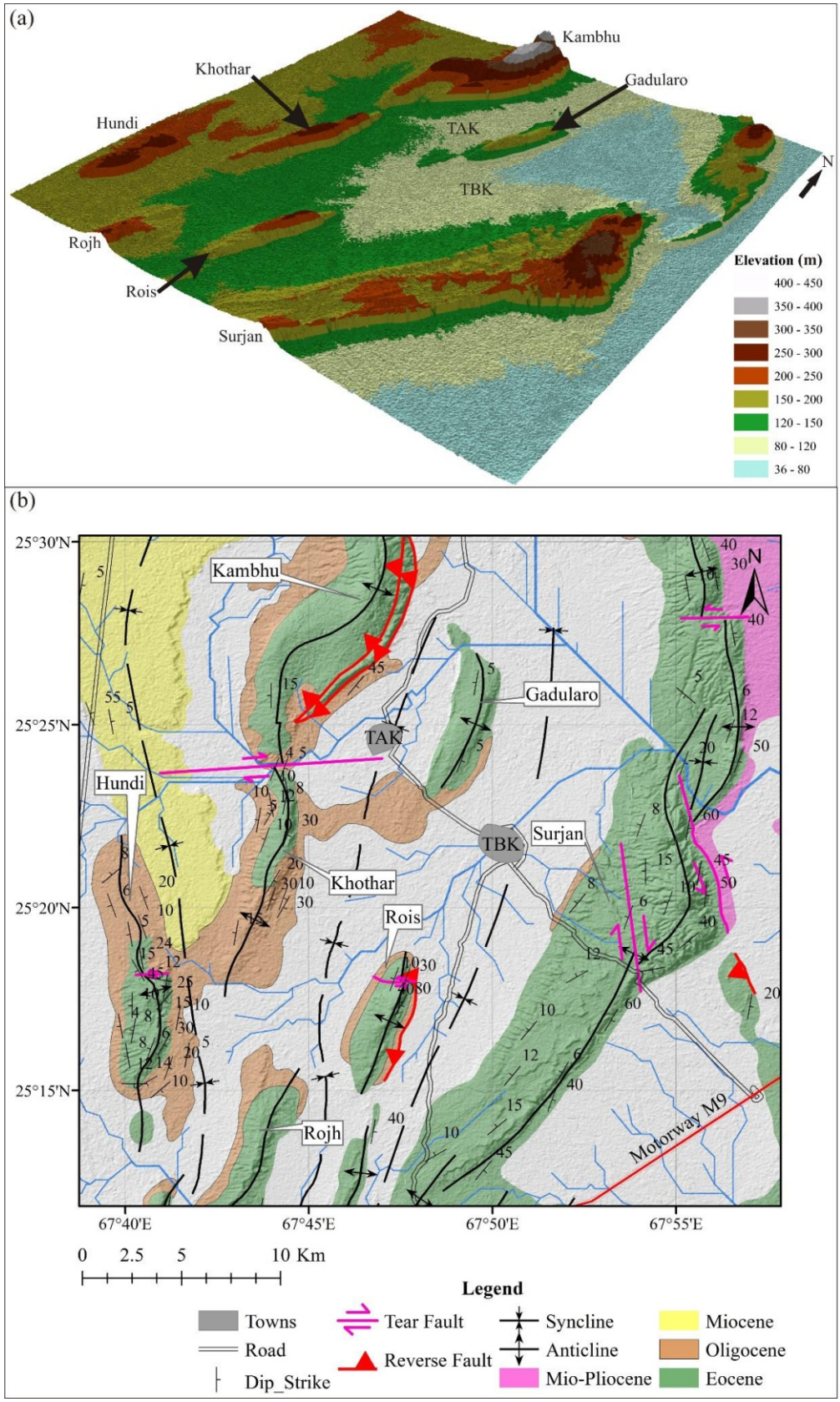

Fig. 2. (a) Hillshade view showing elevation and spatial arrangement of the anticlines in study area, (b) Geological map, showing exposed stratigraphy and structures in the study area. The location of this figure is indicated with red square in figure 1. (TAK=Thano Ahmed Khan town, TBK=Thano Bula Khan town).

3. Materials and Methods

A systematic fieldwork of the Rois anticline was carried out to observe outcrop pattern, collect structural data, particularly dip/strike, fault planes and axis orientation, through brunton compass and the location of each data point was determined using Global Positioning System (GPS). The Frontal thrust of the Rois anticline was identified on the basis of sub-vertical beds of the Nari Formation in the hanging-wall separated by its sub-horizontal beds in the foot-wall in the eastern limb of anticline. However, the Nari Formation in foot-wall is generally covered with Holocene deposits, and it is only identifiable in the drainage channels. Tear fault, bounding frontal thrust in north, was identified on the basis of stratigraphic separation, offset in the fold axis and presence of surface rupture (Figure 3-4). The geological map of Hunting Survey Corporation (1960) was up-scaled (to 1:10,000) and used as reference map to verify stratigraphic contacts and plot structural data. High-resolution field photographs of different field features were captured to aid the collected data. The structural data and faults were plotted on the geological map, using ArcGIS software, to visualize spatial structural pattern and fold-fault relationship in the Rois anticline. Dip/strike data from four different along-strike parts of the anticline were plotted on the lower hemisphere of Schmidt stereonet to construct beta diagrams of each section (Halepoto et al., 2022). The beta-diagrams are very important to understand the geometries of the geological structures and regional stress fields.

We extracted, processed and analyzed lineaments of the Rois anticline, from Digital Elevation Modal (DEM) of "Advanced Land Observing Satellite Phased Array type L-band Synthetic Aperture Radar (ALOS PALSAR)" having spatial resolution of 12.5m. Fractures or lineaments can be mapped either in the field or using remote-sensing techniques. Field-based fracture/lineament mapping could be easier and viable, where fractures are mesoscopic and effects of weathering and erosion are minimal. The weathering and erosion may convert the fractures into deep fissures and steep-walled valleys, therefore field-based fracture/lineament mapping is not a promising option and may lead to invalid conclusions. The fractures of the Rois anticline are converted to broader and steep-walled valleys by weathering and erosion. Therefore, we employed remote-sensing technique for lineaments analysis and their tectonic interpretation. Hillshade images from ALOS PALSAR DEM were prepared in ArcMap at six different sun azimuths and elevation angle without vertical exaggeration (Table 1). These images were than imported into PCI Geomatica software sequentially, where lineaments were extracted automatically using "Line algorithm" tool. The extracted lineaments were than imported into ArcMap interface, to analyze their spatial inter-relationship, relationship with fold and variation in lineaments from one hillshade image to other. The extracted lineaments were than combined in a single shapefile, where duplicate lineaments were removed. Lineament density map and lineament rose diagram were prepared from combined shapefile through ArcMap and Rockworks softwares, respectively. The lineaments were than classified and interpreted according to their relationship with fold axis.

4. Results and Discussion

4.1. Fold Geometry

Outcrop observations indicate that the Rois anticline is about 6.5Km along and 02Km across strike, N-S trending, doubly-plunging, culminated anticline, having steep eastern and gentle western limbs (Figure 3-4). It is capped by Early Eocene Laki Formation, whereas, Oligocene Nari Formation is exposed at both limbs of the anticline (Figure 3-4). The dip values of eastern limb vary from 20° to 80° with an average of 50°, striking towards 010 to 090 azimuths, as per right-hand rule (Figure 4). The dip value of western limb ranges between 04° to 10° with an average of 07°, striking towards 150 to 240 azimuths (Figure 4). Besides east and west dipping limbs, northern and southern parts of the anticline have three-way dip direction (Figure 3-4). The northern part dipping towards N, NE and NW, whereas, southern part dipping towards S, SE and SE directions. Therefore, Rois anticline has four-way dip enclosure, which make it an ideal example of trapping structure. The dip of fore

-limb become steep to sub-vertical at the mapped fault plane of frontal thrust (Figure 3-4). Fold-fault relationship indicates that, the Rois anticline is developed above propagating thrust fault, therefore it is interpreted as fault-propagation fold. The frontal thrust fault is bounded by emergent lateral ramp (tear fault) in the north and become blind southward (Figure 4).

Table 1: Sun azimuth, elevation angle and vertical exaggeration parameters used to create respective hillshade images.

Image No.	Sun Azimuth Angle	Sun Elevation Angle	Vertical Exaggeration
1	045	45	1
2	090	45	1
3	315	15	1
4	315	30	1
5	315	45	1
6	315	60	1

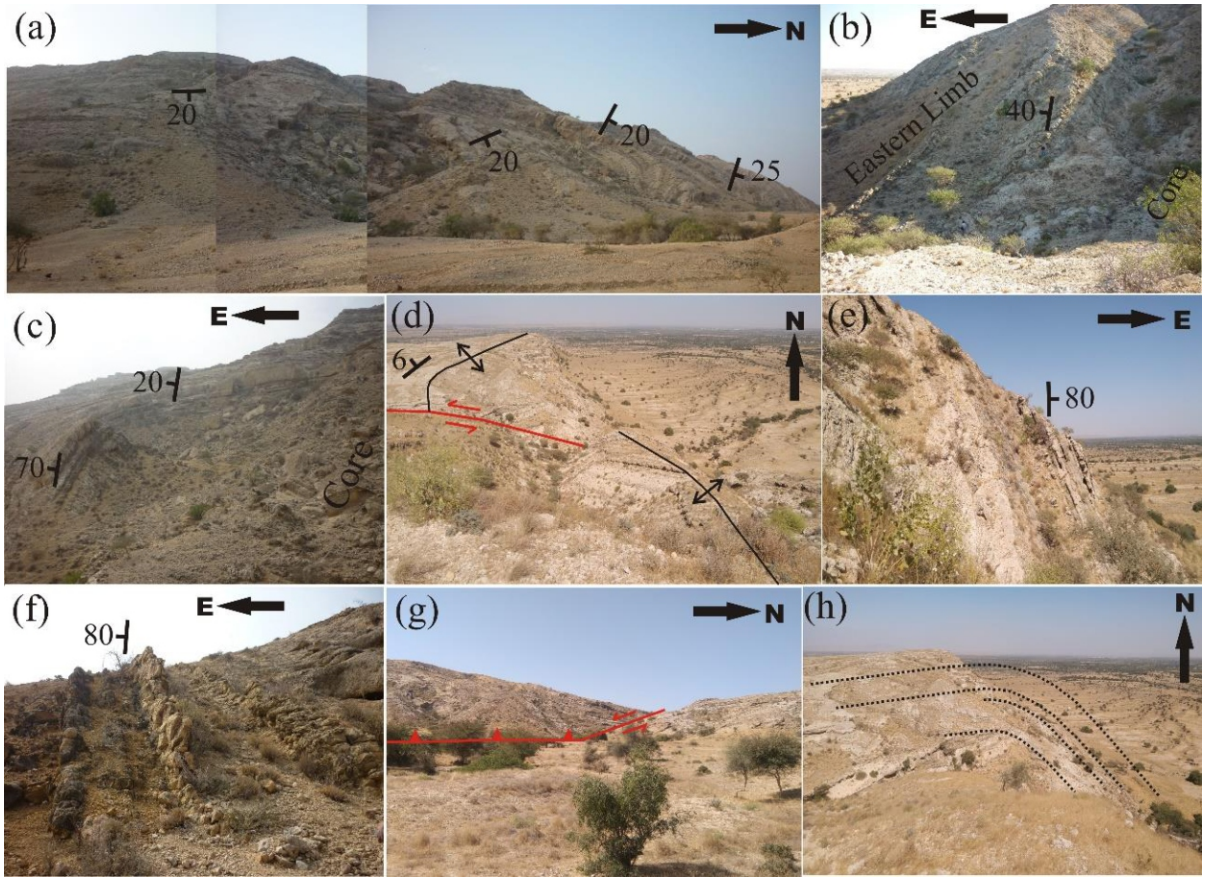

Fig. 3. Field photographs of the Rois anticline, (a) Dip trend at northern part of the Rois anticline, (b-c) Core and eastern limb, (d) View from the axis, showing tear fault and axis offset along it, (e-f) sub-vertical dip of the eastern limb, (g) distant view of tear fault and frontal thrust, (h) View from the axis, showing that mostly eastern limb is eroded. All field photographs are showing limestone of Laki Formation (Early Eocene) except "f", which shows limestone of Nari Formation (Oligocene).

Table 2: Stereographic projection calculations of the Rois anticline, SKFB, Pakistan.

Structural Data		Location 1	Location 2	Location 3	Location 4
Fold limbs	**Eastern limb (L1)**	020/30	030/80	010/40	030/60
	Western limb (L2)	230/8	220/08	200/06	200/08
	Classification	Asymmetrical	Asymmetrical	Asymmetrical	Asymmetrical
Fold Axis	**Plunge (Degrees)**	3	1.5	1	1.5
	Trend/360	025	030	011	209
	Classification	Horizontal	Horizontal	Horizontal	Horizontal
Axial Plane	**Dip (Degrees)**	79	54	73	64
	Strike/360	206	211	191	206
	Classification	Upright	Inclined	Upright	Inclined
Interlimb Angle	**Degrees/180**	142	92	134	113
	Classification	Gentle	Open	Gentle	Open
Vergence/360	**Azimuth**	116	120	102	120
	Classification	ESE-vergent	ESE-vergent	ESE-vergent	ESE-vergent

Representative dip/strike values from the opposite limbs, at four different along-strike positions, were selected to prepare beta-diagram to visualize fold geometry (Table 2; Figure 4), where location 1 is the northern-most and location 4 is southern-most, with location 3 and location 4 in between. At location 1, fold axis of the anticline plunges at 03° towards 025 azimuths. Axial plane of the anticline is dipping at 79° and striking to 206 azimuths, as per right-hand rule. The anticline has an interlimb angle of 142° at location 1, measured along the profile plane between opposite limbs. Fold vergence is believed to be perpendicular to strike of the axial plane and opposite to its dip direction. It is plotted as pole to the axial plane on the stereonet, therefore azimuth of fold vergence at location 1 is 116.

Fold axis plunges at 1.5° towards 030 azimuths at location 2. Axial plane of the anticline is dipping at 54° and striking to 211 azimuths. The anticline has an interlimb angle of 92° and azimuth of fold vergence is 120 at location 2. Geometrical parameters of location 2 indicates that axial plane become gentler and interlimb angle become tighter than location 1. This is because more tightness in folding at location 2 due to emergent frontal thrust, whereas location 1 is out of thrust-tear fault boundary. At location 3, fold axis plunges 01° towards 011 azimuths. Axial plane of the anticline is dipping at 73° and striking to 191 azimuths. The anticline has an interlimb angle of 134° and fold vergence towards 102.

Fold axis plunges at 1.5° towards 209 azimuths at location 4. Axial plane of the anticline is dipping at 64° and striking to 206 azimuths. The anticline has an interlimb angle of 113° and fold vergence is 120 at location 4. Trend of fold axis plunges and strike of the axial planes confirmed that, these are parallel in all four selected locations of the anticline (Table 2; Figure 4).

The fold geometrical parameters, i.e. fold axis, axial plane, interlimb angle and fold vergence, calculated through stereonet, are used to classify the Rois anticline. The calculated plunge of the fold axis ranges from 1° to 3° towards 011 to 209 azimuth, which indicates that the Rois anticline is a doubly-plunging anticline. The dip/strike of the axial plane of the Rois anticline varies from 211/54° to 206/79°, which indicates that the Rois anticline is inclined to upright asymmetrical anticline. The interlimb angle ranges between

92° to 142°, therefore, the Rois anticline can be classified as gentle to open fold on the basis of interlimb angle. The azimuth of fold vergence ranges from 102 to 120, which indicate that the Rois anticline is ESE vergent anticline. Therefore, Rois anticline is classified as a doubly-plunging, inclined to upright, asymmetrical, gentle to open and ESE-vergent anticline.

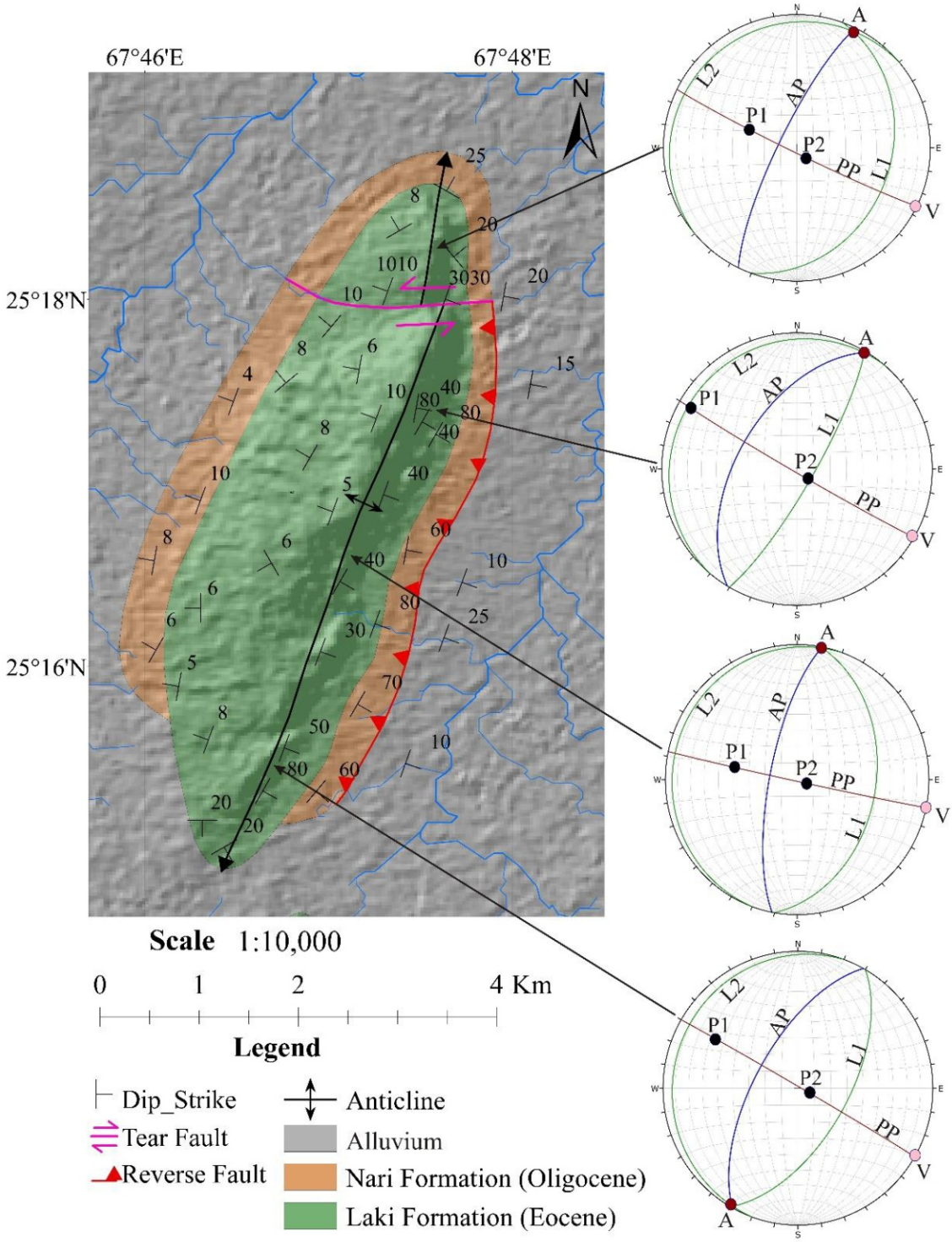

Fig. 4. Geological map, with Beta-diagrams depicting structural geometry of different segments of the Rois anticline, as indicated by arrows. (L1=Limb 1, L2=Limb 2, P1=Pole to limb 1, P2=Pole to limb 2, AP=Axial Plane, PP=Profile Plane, A=Plunge and trend of axis, V=Vergence).

Doubly-plunging geometry of the Rois anticline resulted in canoe-shaped structural style. These types of structural style of the anticlines are common in foreland fold belts, where along-strike variations in fault-propagation and associated lateral shortening produce such three-dimensional fold geometries (Tavani et al., 2015; Jadoon et al., 2020; Rehman et al., 2022; Smeraglia et al., 2024). The doubly-plunging geometry and four-way dip enclosure indicates three-dimensional strain accommodation, suggesting that the deformation was not purely cylindrical. The development of such structural styles could be associated with spatial and temporal variations in the mechanical properties, thickness and rheology of sedimentary rock layers, which controlled the fault-propagation over geological time (Al-Mahmoud et al., 2009; Plašienka et al., 2018; Ji and Li, 2020; Bahrami et al., 2024).

Inclined to upright and asymmetrical attitude of the Rois anticline further confirms the field observations of fault-related folding, where eastern limb steepened in the hanging-wall of propagating thrust fault. Steepening of eastern limb in the hanging-wall of frontal thrust suggests that the anticline has experienced significant eastward tilting (Figure 5a) during its course of development (Al-Kubaisi and Barno, 2015; Tavani et al., 2017; Jadoon et al., 2020; Halepoto et al., 2023b).

Gentle to open fold nature with relatively larger interlimb angle of the Rois anticline suggest early stage of fold development and low-degree of fold tightness. Gentle to open fold geometry of the Rois anticline could be associated with distribution of compressional forces over a broader area of SKFB, which leads to low-amplitude anticlines separated by broad synclines. Furthermore, relatively larger interlimb angle of the Rois anticline could be a result of steep frontal thrust fault, where anticline has experienced combined horizontal and vertical shortening (Figure 5b) (Twiss, 1988; Welbon and Butler, 1992; Thorbjornsen and Dunne, 1997; Li et al., 2018; Nabavi and Fossen, 2021; Joudaki et al., 2024). Folds developed above low-angle propagating thrust faults generally experience dominant horizontal shortening, therefore, tend to have lower interlimb angles (Sengupta et al., 2005; Jabbour et al., 2012; Nabavi and Fossen, 2021; Zhou et al., 2024).

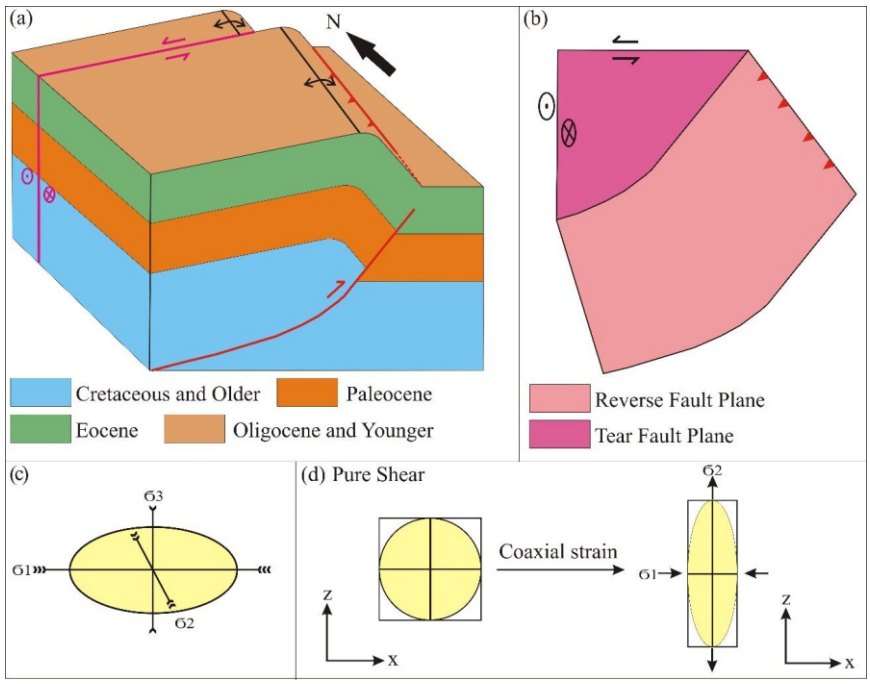

Fig. 5. (a) Block diagrams showing interpreted model of the Rois anticline, (b) Interpreted fault planes of emergent frontal thrust and northern tear fault, (c) Stress ellipsoid showing orientations of principle stress axes during folding, (d) Stress-strain kinematics of the Rois anticline on the basis of outcrop observations.

The ESE vergence of the Rois anticline indicates the regional transport direction towards the east-southeast. This vergence direction of the anticline aligned well with structural alignment of the Kirthar Fold Belt and regional tectonic framework, where compressional forces are generated by the ongoing oblique collision of the Indian and Eurasian plates in the west of the study area (Figure 5c) (Schelling, 1999; Bannert et al., 2014; Hinsch et al., 2019; Ghani et al., 2023; Muhammad et al., 2024; Salam et al., 2024; Ahmedani et al., 2024). The consistency in the trend and vergence of the Rois anticline with regional structural trend and transport direction suggest that it is the product of EW-aligned pure shear and coaxial strain (Figure 5d).

4.2. Lineament Analysis

During the process of lineament extraction, we identified 202 lineaments from six hillshaded DEMs (Figure 6). The total lineaments extracted from each hillshaded DEM, their percentage to total lineaments population, minimum, maximum and average length of lineaments and their class per each hillshaded DEM is given in Table 3 (Figure 7).

We extracted 44 lineaments from hillshade image of 045/45, with an average length of 645m. Generally, these lineaments are transverse and shortest lineaments identified during present study. Most of these lineaments are identified in the back-limb of anticline culmination, however, some lineaments also occur in the hinge area and fore-limb (Figure 7). The remaining five hillshade images yielded generally longitudinal lineaments in the range of 30-33, with average length range of 705-767m. These lineaments are parallel to fold axis and emergent frontal thrust, therefore they are classified as longitudinal lineaments. The hillshade image of 090/45 azimuth and elevation angle yielded longest lineaments in the Rois anticline during present study (Table 3). All extracted lineaments are merged in a combined map and lineament density map is prepared from them (Figure 8a-b). The combined lineament map indicates predominance of longitudinal lineaments (Figure 8a-c). Mostly, longitudinal lineaments are concentrated in the hinge zone of the Rois anticline and only few lineaments are identified in its limbs (Figure 7-8).

The Rois anticline is presently interpreted as doubly-plunging anticline having four-way dip enclosure, therefore, it must have experienced outer-arc extension during its development. This outer-arc extension resulted in the highest central part (culmination) of the anticline. The dominant concentration of transverse lineaments in the culmination of the Rois anticline confirm its outer-arc extension. The outer-arc extension of the anticline is possible where maximum and intermediate stress axes (σ_1 and σ_2) are horizontal, and intermediate stress axis (σ_2) is essentially extensional in relation to compressional maximum stress axis (σ_1) (Figure 5c-d and 8d).

The longitudinal lineaments are developed due to fold-parallel stretching in high-strain parts of the Rois anticline during its development (Figure 8d). These lineaments could be folding-related fracture planes or minor faults, which accommodated the strain along the axial plane of the anticline (Price and Cosgrove, 1990; Price, 2016; Wajid et al., 2021). The identified lineaments could also be manifestation of fault-propagation folding, where slip along the growing fault has been transmitted upward along the anticlinal axial plane, thereby producing fold and fold-related fractures and minor faults (Casini et al., 2018; Wajid et al., 2021; Joudaki et al., 2024). The dominance of longitudinal lineaments (Figure 8c) indicates that compressional forces played a predominant role in shaping the Rois anticline, where folding resulted from fault-propagation (Khan et al., 2007; Yaseen et al., 2021). The fault-propagation folding is also supported by the asymmetry of the anticline, where steep to sub-vertical eastern limb is underlain by emergent frontal thrust, which is responsible for formation of the Rois anticline.

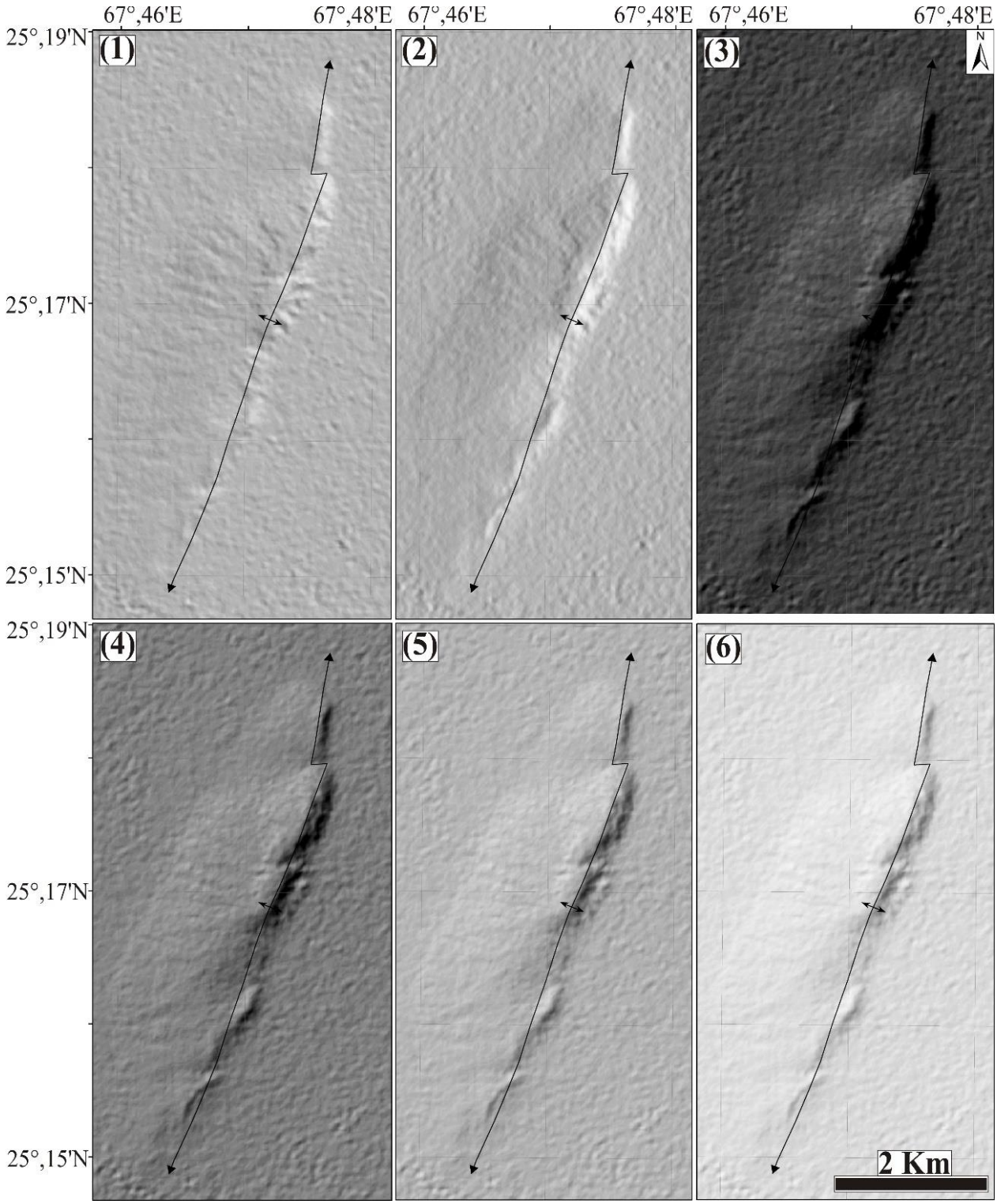

Fig. 6. DEMs of the Rois anticline, hillshaded at different sun azimuths and elevation angles as indicated in Table 1.

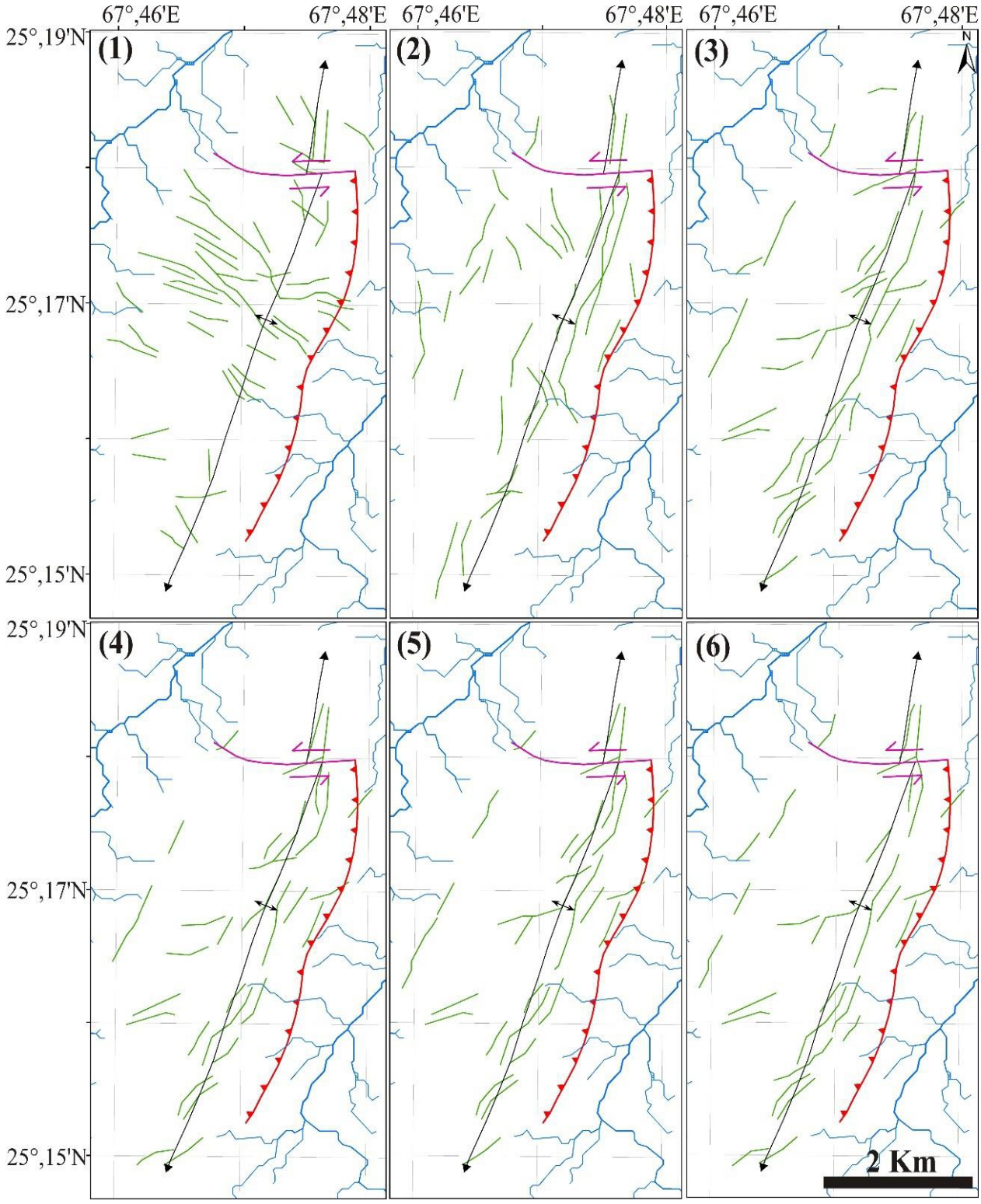

Fig. 7. Lineaments extracted from each respective hillshaded image (as indicated in Figure 6). The lineaments are plotted against fold axis, faults and drainage pattern to visualize their inter-relationship.

Table 3: Total identified lineaments, their percentage to total population, length and class per each hillshaded DEM.

Lineaments Extracted from	Total Lineaments Detected	Percent to Total Population	Length of Lineament (m)			Dominant Class of Lineaments
			Minimum	Maximum	Average	
Hillshade 045/45	44	22	392	1904	645	Transverse
Hillshade 090/45	33	16	375	3089	767	Longitudinal
Hillshade 315/15	33	16	392	1773	741	Longitudinal
Hillshade 315/30	31	15	400	1494	705	Longitudinal
Hillshade 315/45	31	15	392	1742	707	Longitudinal
Hillshade 315/60	30	15	395	1864	720	Longitudinal
Total Population	202	100	375	3089	721	Longitudinal
Duplicate Lineaments	15	7	400	1490	704	Longitudinal
Total	187	93	375	3089	723	Longitudinal

4.3. Regional Tectonic and Kinematic Significance

The outcrop observations and lineament analysis provided significant insights into the regional tectonic and kinematics of the study area. The development of the Rois anticline is ultimately linked to the oblique collision of the Indian Plate and Afghan Block. The anticline has accommodated tectonic shortening through folding and underlying fault propagation, as indicated by the fold-fault relationship. The Rois anticline is a small-scale anticline, therefore its development could be attributed to localized strain partitioning in the study area. The localized strain partition is accommodated by the flexural slip and folding. Despite being located adjacent to NS-trending, left-lateral convergent wrenching regime of the Ornach-Nal and Chaman plate boundary, no strike-slip faulting parallel to plate boundary is observed in study area. It indicates significant strain partitioning along the Ornach-Nal and Chaman plate boundary, where left-lateral deformation has been accommodated and is not transmitted to foreland (Schelling, 1999; Ghani et al. 2023). The strike-slip deformation is restricted within the hinterland and is manifested by seismically active faults, whereas, dip-slip compressional deformation is transmitted to the foreland (Khan et al., 2011; Szeliga et al., 2012; Hinsch et al., 2019). Therefore, the Rois anticline is interpreted to have developed as a result of compressional pure shear associated with oblique convergence (transpression) between the Indian Plate and Afghan Block along the Ornach-Nal and Chaman plate boundary. The consistency of trend of the Rois anticline with regional structural trend of the Southern Kirthar Fold Belt and transport direction indicates that it is product of the coaxial strain.

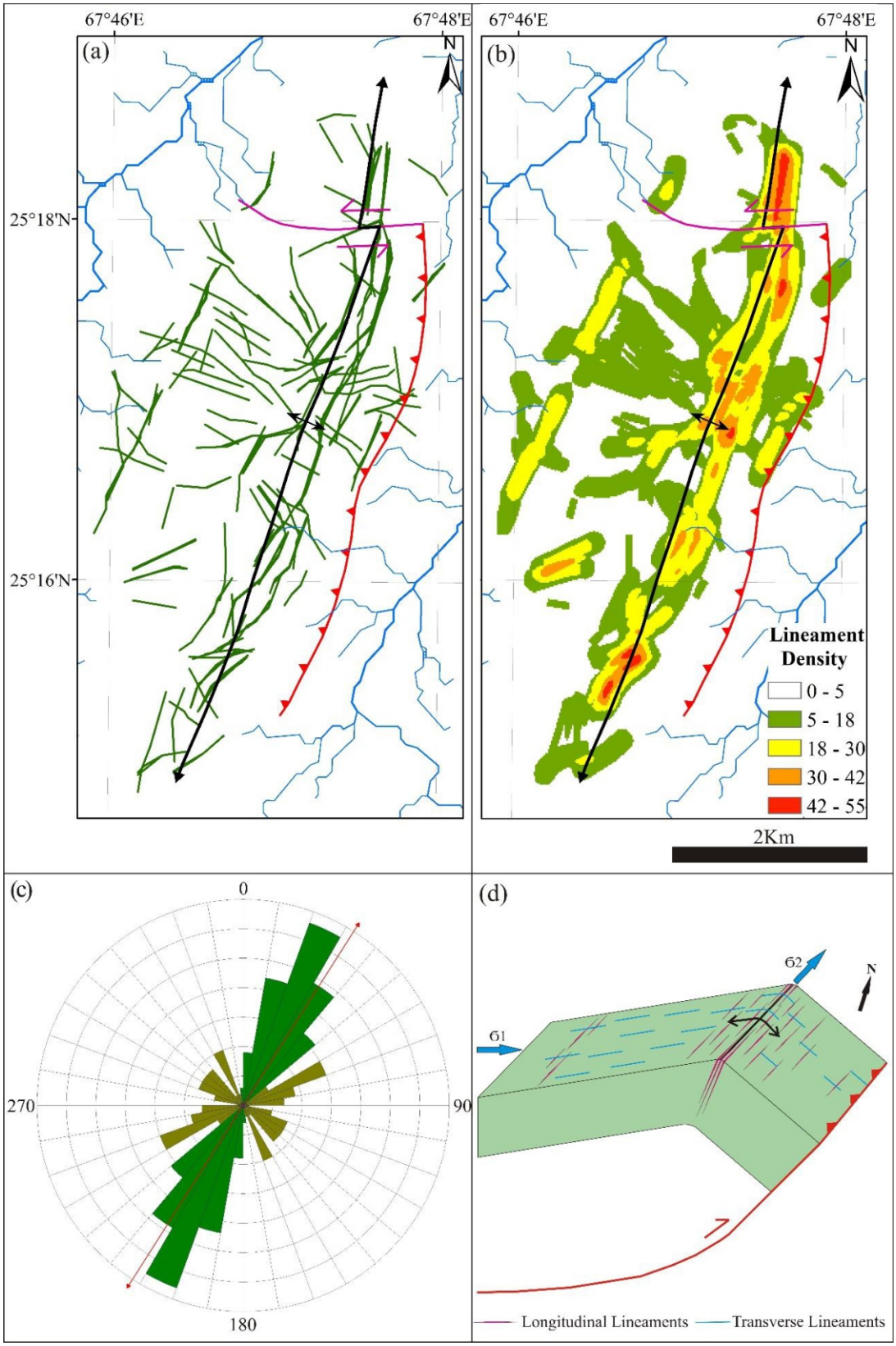

Fig. 8. (a) all lineaments extracted from hillshaded images of different sun azimuth angle are combined and plotted against fold axis, faults and drainage pattern of the Rois anticline, (b) Lineament density map indicating number of lineaments per square kilometer, (c) Rose diagram showing orientation of longitudinal lineaments (Green) and transverse lineament (Martian), (d) Schematic diagram of the fault-propagation fold showing lineament distribution pattern in the Rois anticline.

5. Conclusions

The Rois anticline is about 6.5Km along and 02Km across strike, N-S trending , having four-way dip enclosure. It is bounded by emerg ent frontal thrust fault in the eastern limb and lateral ramp (tear fault) along the northern part. Geometrical parameters of the Rois anticline suggest that it is a doubly-plunging, culminated, inclined to upright, asymmetrical, gentle to open and ESE-vergent, having steep eastern and gentle western limbs.
The transverse and longitudinal lineaments are identified in the Rois anticline. Transverse lineaments occur in the culmination, indicating anticline has experienced outer-arc extension. The longitudinal lineaments are concentrated in hinge area of the Rois anticline, which indicate fold-parallel stretching in its high-strain parts. The development of the Rois anticline is linked to the oblique collision of the Indian Plate and Afghan Block along the Ornach-Nal and Chaman plate boundary. The Rois anticline has accommodated localized coaxial strain partitioning, associated with regional pure shear.

Authors Contribution

Aijaz Ali Halepoto; Conceptualization, data curation, formal analysis and writing–original draft preparation. Muhammad Hassan Agheem; Supervision, project administration, methodology, and validation. Asghar A. A. D. Hakro; Visualization, supervision, investigation and writing–review and editing Shabeer Ahmed; Project administration, resources, software and validation. Surriya Bibi Ahmedani; Data curation, formal analysis, writing–original draft preparation.

Acknowledgement

University of Sindh, Jamshoro is highly acknowledged for providing transportation facility to carry out geological fieldwork of study area. We are highly thankful to Chief Editor and editorial board of the Journal of Himalayan Earth Sciences, for effectively handling our manuscript. Authors pay gratitude to anonymous peer-reviewers of this paper, whose critical review, comments and suggestions helped us to enhance quality and outlook of the paper. Authors are also thankful to Wildlife Department, Government of Sindh, for providing guiding and security personnel. We are thankful to Mr. Aitbar Ali Dahani, field driver of Centre for Pure and Applied Geology, for their contribution in the fieldwork. Authors also acknowledge field assistance by students of BS. Geology 2K20 and 2K21 batches.

Conflict of Interest

Authors have no conflict of interest to disclose.

References

Ahmed, R., & Ali, S. M. (1991). Tectonic and structural development of the Eastern Kirthar fold belt and its hydrocarbon prospects. *Pakistan Journal of Hydrocarbon Research*, *3*, 19–31.

Ahmedani, S. B., Agheem, M. H., Hakro, A. A. A. D., Halepoto, A. A., Lashari, R. A., & Thebo, G. M. (2024). Integrated petrographical, mineralogical, and geochemical investigation to evaluate diagenesis of sandstone: A case study of the Oligocene Nari formation from Southern Kirthar Range, Pakistan. *Journal of Himalayan Earth Sciences*, *57*(1), 1–22.

Al-Kubaisi, M. S., & Barno, J. M. (2015). Fold geometry and kinematics of inversion tectonics for Kosrat anticline, northeastern Iraq. A*rabian Journal of Geosciences*, *8*, 9469–9480.

Al-Mahmoud, M. J., Khalil, M. H., & Moustafa, A. R. (2009). The Jinadriyah anticlines: A surface model for oil fields in eastern Saudi Arabia. *Arabian Journal of Geosciences*, *2*, 213–234.

Allemann, F. (1979). Time of emplacement of the Zhob Valley ophiolites and Bela ophiolites, Baluchistan (Preliminary report). In A. Farah & K. A. DeJong (Eds.), *Geodynamics of Pakistan* (pp. 215–242). Geological Survey of Pakistan.

Bahrami, S., Ehteshami-Moinabadi, M., & Tuyserkani, M. S. (2024). Quantitative evaluation of morphometric parameters of drainage system in the forelimb and backlimb of the Asmari anticline, Zagros, Iran. *Journal of Structural Geology*, *184*, 105151.

https://doi.org/10.1016/j.jsg.2024.105151

Banks, C. J., & Warburton, J. (1986). "Passive-roof" duplex geometry in the frontal structures of the Kirthar and Sulaiman Mountain belts, Pakistan. *Journal of Structural Geology*, *8*, 229–237.

Bannert, D., Cheema, A., Ahmed, A., & Schaffer, U. (1992). The structural development of the Western Fold Belt, Pakistan. *Geologisches Jahrbuch Reihe*, *B80*, 3–60.

Bannert, D., Iqbal, M., & Khan, M. R. (2014). The architecture of the Northwestern Indian plate collision zone. *Pakistan Journal of Hydrocarbon Research*, *24*, 1–17.

Butler, R. W. H., Bond, C. E., Cooper, M. A., & Watkins, H. (2018). Interpreting structural geometry in fold-thrust belts: Why style matters. *Journal of Structural Geology*, *114*, 251-273. https://doi.org/10.1016/j.jsg.2018.06.019

Casini, G., Romaire, I., Casciello, E., Saura, E., Vergés, J., Fernández, N., & Hunt, D. W. (2018). Fracture characterization in sigmoidal folds: Insights from the Siah Kuh anticline, Zagros, Iran. *AAPG Bulletin*, *102*, 369–399.

De Jong, K. A., & Subhani, A. M. (1979). Note on the Bela ophiolites, with special reference to the Kanar area. In A. Farah & K. A. DeJong (Eds.), *Geodynamics of Pakistan* (pp. 263–269). Geological Survey of Pakistan.

Erslev, E. A., & Mayborn, K. R. (1997). Multiple geometries and modes of fault-propagation folding in the Canadian thrust belt. J*ournal of Structural Geology*, *19*, 321–335.

Fowler, J. N., Graham, R., Smewing, J. D., Warburton, J., & Sassi, W. (2004). Two-dimensional kinematic modeling of the Southern Kirthar Fold Belt, Pakistan. In R. Swennen, F. Roure, & J. W. Granath (Eds.), *Deformation, fluid flow, and reservoir appraisal in foreland fold and thrust belts* (pp. 117–131). American Association of Petroleum Geologists. https://doi.org/10.1306/1025688H13112

Ghani, H., Hinsch, R., Sobel, E. R., & Glodny, J. (2023). Oligocene to Pliocene structural evolution of the frontal Kirthar fold and thrust belt of Pakistan. *Journal of Structural Geology*, *176,* 104961. https://doi.org/10.1016/j.jsg.2023.104961

Ghani, H., Sobel, E. R., Zeilinger, G., Glodny, J., Irum, I., & Sajid, M. (2021). Spatio-temporal structural evolution of the Kohat fold and thrust belt of Pakistan. J*ournal of Structural Geology*, *145*, 104310. https://doi.org/10.1016/j.jsg.2021.104310.

Gupta, R.P. (2018). Introduction. In: *Remote Sensing Geology*. Springer, Berlin, Heidelberg. 10.1007/978-3-662-55876-8_1

Halepoto, A. A., Agheem, M. H., Wahid, S., Hakro, A. A. A. D., Lashari, R. A., & Ahmedani, S. B. (2022). Structural analysis of the Ranikot anticline, Southern Kirthar Fold Belt, Pakistan. *Sindh University Research Journal (Science Series)*, *54*, 21-27. https://doi.org/10.26692/surj-ss.v54i04.4350

Halepoto, A. A., Agheem, M. H., Lashari, R. A., Hakro, A. A. A. D., & Ahmedani, S. B. (2023a). Development and synclinal-anticlinal breakthrough of fault-propagation fold: Insights from Borr Dhoro section of the Ranikot anticline, Southern Kirthar Fold Belt, Pakistan. *Sindh University Research Journal (Sciences Series)*, *55*, 32-41. https://doi.org/10.26692/surj-ss.v55i01.4179

Halepoto, A. A., Ahmed, S., Agheem, M. H., Hakro, A. A. A. D., Lashari, R. A., & Ahmedani, S. B. (2023b). Integrated study of structural styles and their suitability for hydrocarbon entrapment, Southern Kirthar Fold Belt, Pakistan. J*ournal of Physics: Conference Series*, *2594*, 1-2. https://doi.org/10.1088/1742-6596/2594/1/012021

Halepoto, A. A., Ahmed, S., Agheem, M. H., Hakro, A. A. A. D., Lashari, R. A., & Ahmedani, S. B. (2023c). Assessment of suitability for hydrocarbon entrapment in the Ranikot anticline, Southern Kirthar Fold Belt (SKFB), Pakistan. *PAPG-SPE Annual Technical Conference-2022*, 35–48.

Hedley, R., Warburton, J., & Smewing, J. (2001). Sequence stratigraphy and tectonics in the Kirthar foldbelt, Pakistan. *PAPG/SPE Annual Technical Conference*, 7-8 November 2001, Islamabad, Pakistan.

Hinsch, R., Asmar, C., Nasim, M., Abbas, M. A., & Sultan, S. (2019). Linked thick- to thin

skinned inversion in the central Kirthar Fold Belt of Pakistan. *Solid Earth*, *10*, 425–446. https://doi.org/10.5194/se-10-425-2019

Hunting Survey Corporation. (1960). *Reconnaissance geology of part of West Pakistan*. A Colombo Plan Co-operative Project.

Jabbour, M., Dhont, D., Hervouët, Y., & Deroin, J. (2012). Geometry and kinematics of fault-propagation folds with variable interlimb angle. *Journal of Structural Geololgy*, *42*, 212-226 https://doi.org/10.1016/j.jsg.2012.05.002

Jadoon, I. A. K., Ding, L., Nazir, J., Idrees, M., & Jadoon, S. ur R. K. (2020). Structural interpretation of frontal folds and hydrocarbon exploration, western Sulaiman fold belt, Pakistan. *Marine and Petroleum Geology*, *117*, 104380. https://doi.org/10.1016/j.marpetgeo.2020.104380

Jadoon, I. A. K., Hinderer, M., Wazir, B., Yousaf, R., Bahadar, S., Hassan, M., Abbasi, Z. ul H., & Jadoon, S. (2015). Structural styles, hydrocarbon prospects, and potential in the Salt Range and Potwar Plateau, north Pakistan. *Arabian Journal of Geosciences*, *8*, 5111-5125. https://doi.org/10.1007/s12517-014-1566-9.

Jadoon, S. R. K., Ding, L., Jadoon, I. A. K., Razzaq, S. S., Javed, M., Afridi, S., Khan, M. A., Qasim, M., & Cai, F. (2024). Digital elevation model-based lineament analysis of the Zindapir anticline, Sulaiman fold-and-thrust belt, Pakistan. *Geological Journal*, 1-12. http://doi.org/10.1002/gj.4977

Ji, S., & Li, L. (2020). An alternative interpretation for the formation of doubly plunging folds in sandstone terrains. *Terra Nova*, *32*, 325–333.

Jiang, D., Wang, M., Song, G., Yan, B., & Feng, W. (2020). Transition from fault-propagation folds to fault-bend folds determined by along-strike variations of structural styles and fault displacement-distance relationships: The Sumatou anticline, Sichuan Basin, China. *Journal of Structural Geology*, *131*, 103951. https://doi.org/10.1016/j.jsg.2019.103951

Joudaki, M., Faghih, A., Mukherjee, S., Seraj, M., & Soleimany, B. (2024). Structural style & kinematic analysis of deformation in the northern Dezful Embayment, Zagros Fold-Thrust Belt, SW Iran. *Marine and Petroleum Geology*, *107*, 122.

Kazmi, A. H., & Rana, R. A. (1982). *Tectonic Map of Pakistan*. Geological Survey of Pakistan Map Series.

Khan, A., Imran, M., Iqbal, M., & Nazeer, A. (2011). Structural styles and hydrocarbon potential of the western Kirthar Fold Belt. In *PAPG-SPE Annual Technical Conference* (pp. 147–174).

Khan, M. I., Ahmad, S., Khan, A. A., & Ali, A. (2007). Fracture network analysis of Samana anticline: A fault-related fold at the front of Samana Range, Orakzai Agency, NWFP, Pakistan. *Pakistan Journal of Hydrocarbon Research*, *17*, 103–114.

Khattak, S. A., Rehman, G., Ahmad, S., Jan, M. F., Khurshid, S., & Ghani, A. (2017). Deformational style and hydrocarbons trapping mechanism of the sub Himalayan frontal ranges near Fateh Jhang, Punjab, Pakistan. *Journal of Himalayan Earth Sciences*, *50*(1), 1–13.

Li, T., Chen, J., Thompson Jobe, J. A., Burbank, D. W., Cheng, X., Xu, J., Li, Z., Zheng, W., & Zhang, P. (2018). Active bending-moment faulting: Geomorphic expression, controlling conditions, accommodation of fold deformation. *Tectonics*, *37*, 2278–2306.

Mitra, S. (1990). Fault propagation folds: Geometry, kinematic evolution, and hydrocarbon traps. T*he American Association of Petroleum Geologists Bulletin*, *74*, 921–945.

Mosar, J., & Suppe, J. (1992). Role of shear in fault-propagation folding. In K. R. McClay (Ed.), *Thrust Tectonics* (pp. 123–132). Geological Society of London.

Muhammad, B. J. H., Ping, W., Mohabbat, M. J., Patmal, M. H., & Ahmad, I. (2024). Morpho-tectonic and satellite image interpretation for identifying Gardez fault in Afghanistan. J*ournal of Geoscience, Engineering, Environment, and Technology*, *9*, 203–208.

Nabavi, S. T., & Fossen, H. (2021). Fold geometry and folding—a review. *Earth-Science Reviews*, *222*, 103812.

Plašienka, D., Šimonová, V., & Bučová, J.

(2018). Nucleation and amplification of doubly-plunging anticlines: The Butkov pericline case study (Manín Unit, Western Carpathians). *Geologica Carpathica*, *69*, 365.

Price, N. J. (1966). *Fault and joint development in brittle and semi-brittle rock*. (pp. 133-16 4). Pergamon Press, Oxford.

Price, N. J., & Cosgrove, J. W. (1990). *Analysis of Geological Structures*. Cambridge University Press.

Rehman, N.-U., Ahmad, S., Faisal, S., Ullah, S., Azeem, M. W., Siab, A., Ullah, R., Shehzad, K., Javed, S., & Nazir, J. (2022). Structural refinement of the southern Kohat Basin and adjoining areas: Implications for hydrocarbon potential of the Kohat Basin, Pakistan. *Bahria University Research Journal of Earth Sciences*, *7*, 8–19.

Salam, H., Turab, S. A., Ali, A., Jan, M. Q., Sulaiman, N., Basori, M. B. I. (2024). Kahi mélange complex in Kurram and Waziristan, NW Pakistan: An integrated approach for tectonic implications to India–Afghan suturing. *Gondwana Research*, *126*, 79–95.

Sarwar, G. (1992). Tectonic setting of the Bela Ophiolites, southern Pakistan. *Tectonoph ysics*, *207*, 3 5 9 – 3 8 1 . https://doi.org/10. 1016/0040-1951(92)90396-N

Schelling, D. D. (1999). Frontal structural geometries and detachment tectonics of the northeastern Karachi arc, southern Kirthar Range, Pakistan. In A. Macfarlane, R. B. Sorkhabi, & J. Quade (Eds.), *Himalaya and Tibet: Mountain Roots to Mountain Tops* (pp. 287–302). Geological Society of America. https://doi.org/10.1130/0-8137-2328-0.287

Sengupta, S., Ghosh, S. K., Deb, S. K., & Khan, D. (2005). Opening and closing of folds in superposed deformations. *Journal of Structural Geology*, *27*, 1282–1299.

Smeraglia, L., Fabbi, S., Cipriani, A., Consorti, L., Sirna, M., Corbi, F., Pizzati, M., Parotto, M., Cavinato, G. P. (2024). Deformation mechanisms and slip behaviors of tectonically deformed conglomerates from the Central Apennines fold-and-thrust belt: Implications for shallow aseismic and seismic slip. *Journal of Structural Geology*, *186*, 105202.

Smewing, J. D., Warburton, J., Cernuschi, A., & Ul-Haq, N. (2002a). Structural inheritance in the southern Kirthar Fold Belt. *PAPG/SPE Annual Technical Conference*, 22–23 November 2002, Islamabad, Pakistan.

Smewing, J. D., Warburton, J., Daley, T., Copestake, P., & Ul-Haq, N. (2002b). Sequence stratigraphy of the southern Kirthar Fold Belt and Middle Indus Basin, Pakistan. In P. D. Clift, D. Kroon, C. Gaedicke, & J. Craig (Eds.), *The Tectonic and Climatic Evolution of the Arabian Sea Region* (pp. 273–299). Geological Society of London.

Suppe, J., & Medwedeff, D. A. (1990). Geometry and kinematics of fault-propagation folding. *Eclogae Geologicae Helvetiae*, *83*(3), 409–454.

Szeliga, W., Bilham, R., Kakar, D. M., Lodi, S. H. (2012). Interseismic strain accumulation along the western boundary of the Indian subcontinent. *Journal of Geophysical Research*, *117*, 1–14. https://doi.org/10.1029/2011JB008822

Tavani, S., Granado, P., Arbués, P., Corradetti, A., & Muñoz, J.A. (2017). Syn-thrusting, near-surface flexural-slipping and stress deflection along folded sedimentary layers of the Sant Corneli-Bóixols anticline (Pyrenees, Spain). *Solid Earth*, *8*, 405–419.

Tavani, S., Storti, F., Lacombe, O., Corradetti, A., Muñoz, J.A., & Mazzoli, S. (2015). A review of deformation pattern templates in foreland basin systems and fold-and-thrust belts: Implications for the state of stress in the frontal regions of thrust wedges. *Earth Science Reviews*, *141*, 82-104. https://doi.org/10.1016/j.earscirev.2014.11 .013

Tavani, S., Storti, F., & Salvini, F. (2006). Double-edge fault-propagation folding: geometry and kinematics. *Journal of Structural Geology*, *2 8* , 1 9 – 3 5 . https://doi.org/10.1016/j.jsg.2005.09.007

Thebo, G. M., Solangi, S. H., Agheem, M. H., Solangi, M. A., Markhand, A. H., & Memon, K. A. (2023). Petrography and Geochemistry of late Cretaceous Pab Sandstone, Laki range, Southern Indus Basin, Pakistan: implications for Provenance and Paleoclimate. J*ournal of Himalayan Earth Science*s, *56*(1), 65-78.

http://ojs.uop.edu.pk/jhes/article/view/1249.
Thorbjornsen, K.L., & Dunne, W.M. (1997). Origin of a thrust-related fold: geometric vs kinematic tests. *Journal of Structural Geology*, *19*, 303–319.
Twiss, R.J. (1988). Description and classification of folds in single surfaces. *Journal of Structural Geology*, *10*, 607–623.
Wajid, A.A., Anees, M., Alam, S. ul, Gorchani, J.K., Shahzad, K., Israr, A., & Shafique, M. (2021). Lineament mapping for a part of the Central Sulaiman Fold–Thrust Belt (SFTB), Pakistan. *Arabian Journal of Geosciences*, *14*, 1-19. https://doi.org/10.1007/s12517-021-07784-y
Watkins, H., Bond, C.E., Cawood, A.J., Cooper, M.A., & Warren, M.J. (2019). Fracture distribution on the Swift Reservoir Anticline, Montana: Implications for structural and lithological controls on fracture intensity. In: Bond, C.E., Lebit, H.D. (Eds.), Folding and Fracturing of Rocks: 50 Years of Research since the Seminal Text Book of J. G. Ramsay. Geological Society, London.
Watkins, H., Butler, R.W.H., Bond, C.E., & Healy, D. (2015). Influence of structural position on fracture networks in the Torridon Group, Achnashellach fold and thrust belt, NW Scotland. *Journal of Structural Geology*, *74*, 64–80. https://doi.org/10.1016/j.jsg.2015.03.001
Welbon, A.I., & Butler, R.W.H. (1992). Structural styles in thrust belts developed through rift basins: A view from the western Alps, Norwegian Petroleum Society Special Publications. Elsevier B.V. https://doi.org/10.1016/B978-0-444-88607-1.50037-1
Wu, X., Li, Z., Yang, X., Sun, C., Wang, W., Lv, L., & Long, W. (2023). Quantifying and modeling curved thrust fault-propagation folds at different scales. *Journal of Structural Geology*, *172*, 104888. https://doi.org/10.1016/j.jsg.2023.104888
Yaseen, M., Ali Shah, S., Khan, J., Samiullah, A., Jan, A., Sheeraz Khan, M., & Sair, S. (2021). Fracture Analysis and Reservoir Potential of Exposed Eocene Successions Along Kohat-Orakzai Transact Khyber Pakhtunkhwa, NW Pakistan. *Journal of Mountain Area Research*, *6*, 77. https://doi.org/10.53874/jmar.v6i0.121
Zhou, P., Chen, X., Shao, Z., Zhang, Y., Liu, K., Xu, S., Li, B., Xu, D., & Wang, Y. (2024). Differential deformation mechanism of E–W-trending Weiningbeishan fold-thrust belt from central Ningxia, NW China. *Geological Journal*, *59*, 1841–1860. https://doi.org/10.1002/gj.4973